

DENOISING POINT CLOUD DATA OF SMALL-STRUCTURED FREE FORM-SURFACES CAPTURED BY A PHASE-BASED LASERSCANNER

E. Richter

Geodetic Institute, University of Karlsruhe (TH), 76128 Karlsruhe, Germany - richter@gik.uka.de

KEY WORDS: Laser scanning, Close-range, Point Cloud, Filtering, Cultural Heritage

ABSTRACT:

Terrestrial laser scanners based on the time-of-flight measurement principle or the phase comparison method are used for cultural heritage documentation. Only if the scanned surfaces consist of extended, only slightly curved structures, the noise of the point cloud becomes nearly irrelevant as soon as the point cloud is replaced by a parametric or analytic description of the surface. In this paper, the usage of a phase based scanner for capturing small-structured free form surfaces shall be investigated, whereas two procedures are used to reduce the noise of the point cloud: repeated scanning and calculation of average, then smoothing the point cloud with an edge-preserving filter, based on anisotropic diffusion. The physical background of the anisotropic diffusion filter is given, the work-flow is described and the gained results are discussed. It will be seen, that via repeated scanning and usage of an edge-preserving filter good results also in close-range can be achieved with a terrestrial laser scanner based on the phase comparison method.

1. MOTIVATION

1.1 Terrestrial Laser Scanning for Cultural Heritage Documentation

Amongst many other applications, terrestrial laser scanners are used for cultural heritage documentation. 'Terrestrial laser scanner' is a commonly used term for scanners based on the direct time-of-flight measurement of a laser pulse or on the phase comparison method, but also triangulation systems may be included into this term, as shall be done from now on. Mostly it is desirable that the noisy point cloud is replaced by geometric primitives or a free-form surface description using NURBS. With the calculation of average during the estimation of the describing parameters of the geometry via best-fit, the noise effect can nearly completely be eliminated. Edges, which in the original point cloud were rounded and spread, no more distort the results, because the geometric primitives can be extended and intersected, and so sharp edges are achieved again. Problems especially in using pulse or phase based laser scanners occur, when the object has a small-structured free-form surface, as for example hand-crafted reliefs have them (Fig. 1). Here mostly triangulation sensors are preferred to acquire the geometry. But mainly because they offer a much larger field-of-view (FOV), it seems desirable that also pulse- or phase-based scanners are used for close-range-scanning; i.e. Nothegger and Dorninger (2009) show a complete workflow from scanning and calibration to a thinned and smoothed point cloud of a phase based scanner, employed as a close-range scanner. The next section discusses the advantages and disadvantages of pulse, phase and triangulation methods with a special focus on scanning small-structured surfaces.

1.2 Triangulation Methods, Pulse- and Phase based Laser Scanning

1.2.1 3D Triangulation Sensors: One of the advantages of triangulation scanners, based either on white or coloured light pattern projection (mostly fringes) or on laser line projection, is their high resolution; an exemplary value is 0.12 mm for a 0.2 m FOV diagonal (Breuckmann optoTOP-HE). Another advantage is their speed: acquiring the whole FOV in less than one second is possible with a fringe projection system, depending on the number of projected patterns. Laser light section sensors are slower, they need some seconds up to several minutes. The data quality of the triangulation sensors in general is higher than the one of pulse or phase based scanners: the noise only reaches some micrometers (fringe projection systems) up to some ten micrometers (laser light section method). Disadvantages of the triangulation sensors are the narrow FOVs, the non-linearity, which results in short operating ranges of about only 2 m, and the non-coaxiality, which causes shadowing at small-structured surfaces. This causes the dilemma, that either the distance between camera and projector is enlarged to improve the depth resolution but on the other hand get more shadowing, or put camera and projector closer together for being able to look into narrow holes, but lose depth resolution.



Figure 1. Picture (left) and model (right) of the test object. The highest elevation of the relief is 4 cm.

1.2.2 Pulse and Phase Measurement Methods: Phase- or pulse-based Laserscanners have ranges up to some ten metres (phase), respectively kilometres (pulse) with coordinate uncertainties from a few millimetres up to centimetres. Among these two measurement principles, in close-range, the phase-based scanners show better results in range noise behaviour – in a distance of up to 10 m, scanning a cooperative target surface, they can reach remarkable low noise in the order of a few submillimetres (see i.e. Böhler et al. (2003), and section 3.1). Yet compared to the triangulation methods, even the phase method shows deficits when used for close-range scanning, which shall be discussed in the next sections.

Angular Errors: Measured vertical and horizontal angles are results from reading the encoder increments. The angles are affected by systematic effects like the eccentricities of angular encoders, because of a trunnion axis error or because of internal encoder errors. Moreover, random errors occur. For a detailed modelling of angular errors see i.e. Lichti and Licht (2006). Manufacturers try to reduce the systematic errors by exact manufacturing and adding calibration values. Nevertheless the question is, if determinable angular errors as the error of the trunnion axis have to be taken into account for close-range scans. Examinations, i.e. by Lichti and Licht (2006), can give some guideline values. We assumed, that especially the range noise and the extended footprint of the laser beam would cause the largest errors and therefore first focussed on these problems; as long as just a narrow FOV, like the 5x5-degree FOV we had, is scanned, all the pixels inside this FOV will be affected by the similar size of trunnion axis or eccentricity errors.

Range Errors: The measured range is affected by systematic errors like electronic and optical crosstalk and random errors like diode and receiver noise (Amann et al. 2001; Wölfelschneider et al. 2005). Because of the short measuring time of only a few microseconds, the noise cannot be reduced via averaging, as can be done in tachymetric measurements, so that in close-range, in a small FOV, this noise is one of the main influence factors of the measured ranges. Moreover, another systematic effect, which has its cause in the lateral extension of the laser beam appears – the mixed pixel effect: A mixed pixel (Hebert, Krotkov 1992) occurs if the laser spot is distributed on several surface parts with different distances from the scanner (Fig. 2). In fact, certainly each measured point is a mixed pixel, but on a smooth surface, facing the scanner, the effect is not observable. The physical background of the mixed pixel effect, especially the relation between signal properties, surface geometry and reflectance, is discussed in Adams and Probert (1996).

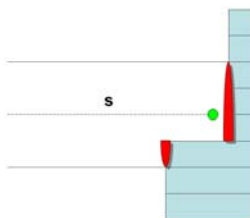


Figure 2. Departed footprint on the object surface, causing a mixed pixel range value s

As can be seen in Fig. 3, due to the mixed pixels effect, two different surface structures of the same width can cause similar behaviour in the range values: the left structure has 90-degree-

edges, the right one is higher but has flatter edges. Both cause similar range profiles, which might – moreover due to the added noise with $\sigma = 1$ mm, not be distinguishable, even if repeated scans are averaged. Due to the fact that the laser beam keeps in motion during each range measurement, an additional spreading of the footprint happens, so that, based on the manufacturer's data of our scanner, finally the footprint has a diameter of about 4 mm in a distance of 5 m. The intensity inside the spot is approximately gaussian-distributed, which means that inside these 4 mm, without concerning other influences like the angle of incidence and the surface reflectance (see i.e. the discussion of the laser range equation in Pfeifer et al., 2007) this footprint causes an effect similar to a convolution of the surface with a gaussian smoothing filter. This means, that edges are rounded and narrow surface parts are flattened.

So, despite a theoretically high resolution of our phase based scanner of 0.5 mm at a distance of 3.5 m (manufacturer's data), the 3 mm diameter of the laser spot on the surface does not allow to distinguish fine structures on the surface, as will also be seen in section 4.3.

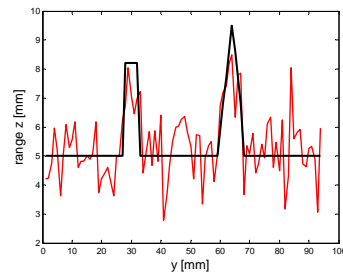


Figure 3. Two different surface structures (black) cause similar range measurement results (red, simulated values).

1.3 Idea

The discussion of the different instrument types gave an overview of their strengths and weaknesses. Although triangulation sensors might be of higher accuracy and resolution in close-range, it might be more practicable, if already a pulse or phase scanner is in use for example to scan the interior of a church, also to scan some smaller objects with the same instrument. In our case, a phase-based laser scanner was used for 'close-range' scanning, which means the object that has to be digitized has a volume of a few cubic decimetres and has highly detailed surface with surface structures of just a few millimetres width on it. To reduce the noise problem, which for this kind of surface cannot be removed by averaging over neighbouring pixels without strongly flattening the fine structures, repeated scans will be made. Nevertheless, the extension of the footprint itself causes flattening, as has been discussed in section 1.2.2. It is not possible to remove the noise completely just by repeated scanning – as Gordon et al. (2003) stated, scanning and averaging at the best improves the standard deviation according to the square root of the number of the scans. So to reduce a noise with $\sigma = 2$ mm (manufacturer's data) down to 0.2 mm, 100 scans must be made. In the meantime, other problems like drift effects may occur, not to talk about the scanning time that would be needed. So the idea was to scan 20 times, achieving a noise with $\sigma \approx 0.4$ mm and afterwards carefully use an edge-preserving smoothing filter. Even this kind of filter will flatten edges, but much less that a gaussian filter for example does (when the same degree of smoothing shall be reached). Moreover, the filter parameters may, after smoothing via

repeated scanning and averaging, be used more carefully, so that on the one hand, a good smoothing effect is achieved and on the other hand the detailed structures are preserved as good as possible. Again it has to be annotated, that an application of the method to objects, which consist of large-volume smooth free form or regular surface elements certainly makes no sense, see section 1.1. In the next section we will have a closer look at the anisotropic diffusion filter, which was implemented for edge-preserving smoothing of the point cloud that had resulted from repeated scanning and averaging.

2. ANISOTROPIC DIFFUSION FOR EDGE-PRESERVING SMOOTHING

2.1 Physical Background

Image denoising via anisotropic diffusion (AD) after Perona and Malik (1990) is a known method in image processing and meanwhile also in point cloud processing, see i.e. Zhang et al. (2006). The AD filter is based on the approach that a noisy image or point cloud during its smoothing process ideally should behave like a thermal field, in which different temperatures will assimilate over time. In case the heat inside a material with a non-uniform temperature distribution just can flow in x -direction (Fig. 4), the heat flux J at the time t , passing a cross-sectional area dividing the material into two volume elements at x , is proportional to the negative temperature gradient at x :

$$J_{x,t} = -\kappa \frac{\partial T_{x,t}}{\partial x} \quad (1)$$

where κ = heat conductivity (material specific parameter)
 T = temperature
 t = time

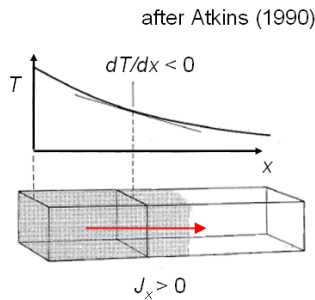


Figure 4. In the left volume element, the temperature is higher than in the right one, so the temperature gradient is negative and the heat flux is positive in x -direction (red).

From this law (Fick's first law of diffusion), the diffusion equation is derived: For a calculation of the overall energy flux over a time span of Δt , one has to know the origin state of the system at time t , $J(x,t)$. Then the sum of all changes that have happened at all times in the interval Δt has to be added. A change or net energy flux at a time t in turn is the sum of all incoming and outgoing energy through the boundary layers at this moment:

$$\frac{\partial J_{x,t}}{\partial t} = \kappa \frac{\partial^2 T_{x,t}}{\partial x^2} \quad (2)$$

Then the final state of the system after the time Δt has passed becomes

$$J_{x,t+\Delta t} = J_{x,t} + \kappa \sum_t^{t+\Delta t} \frac{\partial^2 T_{x,t}}{\partial x^2} \quad (3)$$

What does this equation state? The diffusion equation says, that the higher the temperature difference between two volume elements, the larger becomes the second derivative and the faster the temperatures assimilate, whereas volume elements with similar temperatures assimilate slowly. At the time, when there is no more temperature difference inside the whole material, the second derivatives become zero and so no more energy is flowing.

The next section will show how the heat equation can be used for smoothing noisy images or point clouds.

2.2 Adaptation to Image/Point Cloud Smoothing

How can the diffusion equation be used for smoothing point clouds? When second derivatives of a noisy point cloud are calculated, edges of the geometry cause high derivatives, whereas white noise just causes small derivatives (naturally only if the noise is not larger than the edge heights). So when the diffusion equation shall be adapted to this fact, its effect must be reversed: Where formerly high derivatives caused fast assimilation of temperatures, now high derivatives shall prevent assimilation respectively smoothing, so that edges are not rounded and small structures are not flattened. Small derivatives, however, shall cause fast smoothing, because they are considered to derive from noise. So to adapt the heat equation, the conductivity κ is replaced by a new parameter c , which has to be chosen by the user. Then the heat diffusion equation (Eq. 2) for smoothing images can be written as

$$\Delta z_{x,y} = c \cdot \left[\frac{\partial^2 z}{\partial x^2} + \frac{\partial^2 z}{\partial y^2} \right] = c \cdot \nabla z \quad (4)$$

Now there are two directions, x and y , in which the noise may 'flow', and which are the two directions representing the image matrix. The parameter to be smoothed is z ; this is either the gray-value of an image, or, in our case, the z -coordinate of the point cloud. This simple replacement can be made in case the point cloud may be considered as a 2.5-dimensional problem. Until now, the filter is isotropic: with the parameter c all second derivatives, no matter if large or small, have the same influence on the resulting correction term Δz . In Perona, Malik (1990) several suggestions for c are made, depending on the norm of the gradient. In our case for example, parameter c was chosen as

$$c = \frac{1}{1 + \|\nabla z\|^2} \quad (5)$$

To achieve anisotropic behaviour, a separate smoothing parameter c can be calculated for each of the i.e. four neighbouring pixels, that in x - and y -direction are used (left/right, top/bottom), keeping a common weighting parameter λ to give the user a tool to chose the strength of the AD filter. So finally (4) together with (5) results in the smoothing term

$$\Delta z_{x,y} = \lambda \cdot [c_l \cdot \nabla z_l + c_r \cdot \nabla z_r + c_t \cdot \nabla z_t + c_b \cdot \nabla z_b], \quad (6)$$

which is added to the origin z -value to reduce the noise. Finally edges, where there are large second derivatives, are smoothed much slower than noisy areas. The order of smoothing depends on parameter λ and the amount of iteration steps, both to be chosen by the user. For a closer discussion of anisotropic diffusion see Perona and Malik (1990). Later works, for example Clarenz et al. (2004), altered the method not just to reduce edge smoothing, but even to enhance edges over time.

2.3 Implementation of the AD Filter

There are implementations of AD smoothing filters for unorganized 3D-point clouds, see for example Zhang et al. (2006). In our case, a simplified approach is used: The point cloud is transformed into a new coordinate system, so that afterwards the z -axis is approximately perpendicular to the surface, which causes a nearly equi-distant raster in the existing x - and y -coordinates. Then a second, now indeed equi-distant raster is generated to replace the x - and y -coordinates and the z -values are interpolated to the sampling points of the new raster. From now on, x - and y -coordinates can be treated like an image matrix and the z -coordinates equivalent to a gray-value of an image. Without this interpolation, in a distance of 3.5 m from the scanner and a resolution of 0.55 mm in both directions, a range variation of only 10 cm already causes an angular error of 0.02 mm – per pixel! Over 20 cm, respectively 250 scan lines, this would add up to 5 mm. So even for our relatively 'flat' structure with a maximum elevation of 4 cm, it is necessary to interpolate to equi-distant angle values. Finally, we gain a 'range image', oriented in the x - y -plane, in which the z -values can be smoothed using the AD filter introduced in section 2.2. The disregard of the x - and y -values in the filtering process is derived from the simplification, that the largest part of the range noise appears in the z -value, as long as the object surface is oriented approximately perpendicular to the laser beam.

The next section discusses the improvements that should be achieved by the proposed workflow, consisting of repeated scanning, averaging and filtering.

3. EXPECTED IMPROVEMENTS

3.1 Noise

According to the discussion in section 1.3, repeated measurement of the same point improves the resulting range values, as long as there is just white noise. In a series of tests, comparing scanner ranges to interferometric determined ranges and outliers removed, our scanner showed a noise with $\sigma = 0.4$ mm, when the same point was measured 20 times. According to Gordon (2003), the noise should decrease to $\sigma = 0.2$ mm when the point is measured a hundred times. But opposite to that, the noise increased to $\sigma = 0.8$ mm (Fig. 5) along a distance of 10 m, which might derive from the fact that the pixel was extracted from repeatedly scanned profiles, so that a drift effect may have occurred. Nevertheless, by scanning a surface 20 times, a similar low noise than in the earlier tests could be expected, losing perhaps a bit of it due to the rougher surface of the chosen object and the fact that now 3D- instead of a 2D-scans were made. After the following smoothing of the point cloud via AD filter, a clearly visible improvement, concerning white noise, can be expected.

3.2 Mixed Pixels

The mixed pixel effect can not be reduced by repeated scanning – see the discussion in section 1.2.2. So where the laser footprint is broader than the geometry structure, no improvement by repeated scanning can be expected.

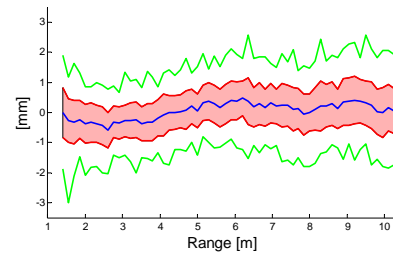


Figure 5. Differences between interferometric ranges and the average of 100 scanner ranges each 0.15 m (blue), band-width of 100 scanner ranges (green) and standard deviations (red).

4. EXPERIMENTAL SETUP, WORKFLOW AND RESULTS

4.1 Experimental Setup

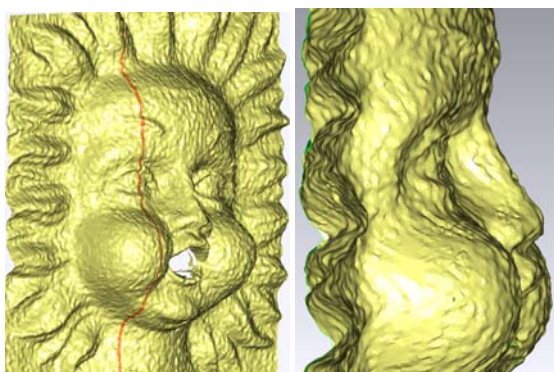
As investigated instrument, a HDS6000 laser scanner was used. The HDS6000 has an ambiguity range of 79 m, the minimum recommended distance to the object is 1 m. Before scanning, the test object (Fig. 1), a 20x20 cm² terracotta relief, was coated with delustering spray to create a surface with homogeneous reflectance properties. Then the object was placed frontal to the scanner, in a distance of about 3.5 m. In this distance, the highest possible angular scanning resolution of both horizontal and vertical 0.009° results in a raster width of 0.5 mm on the object surface. The test object was scanned 20 times. For a verification of the results gained with the HDS6000, additional scans with a light section sensor (Konica-Minolta VI910) were made. The Konica-Minolta VI910 is specified with a point quality of some tenth millimetres (also see Guidi et al. 2007). Point clouds from different viewing angles had to be scanned, mainly because of the shadowing problem discussed in section 1.2.1.

4.2 Data Processing

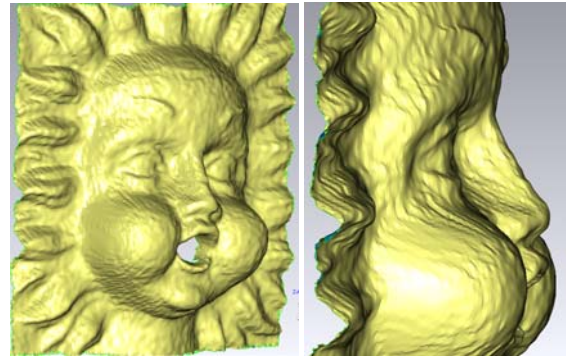
The 20 point clouds from the HDS6000 were exported in the proprietary, binary ZFS-format and afterwards converted into an ASCII-File by using the Z+F-Software Developer Kit (SDK). The SDK contains a c++-File which can be adapted to the user's need; in this case the number of each scan line and pixel, x -, y - and z -coordinates were exported. The ASCII-Files could then be imported into the Matlab-Routines. In Matlab, the averaging routine, transformations and the AD filter were implemented. It took some iterations to find the ideal parameter λ and the ideal amount of iteration steps, which is a general disadvantage of the AD filter compared to simple linear smoothing filters. The point clouds were imported in Geomagic[®], where surface models were calculated (Fig. 6). Afterwards also the scans of the light section sensor were imported in Geomagic[®], then registered and merged, and a surface model was created to serve as reference for the HDS-models.

4.3 Experimental Results

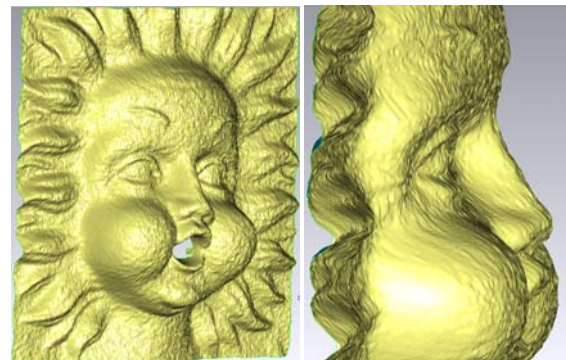
The results of the first part of the described work flow, consisting of scanning the object 20 times with the HDS6000, averaging, and smoothing the point cloud with an AD filter can be seen in Fig. 6: Fig. 6a shows the triangulated mesh of a single scan, without any further processing. The high noise, partially destroying small structures like the eyelids of the figure, is visible. Fig. 6b shows the same scan, this time smoothed using the AD filter and moreover a gaussian filter. The gaussian filter here was needed to remove the strong errors that occurred at the steep edges, for example at the chin. Here the AD filter failed, probably because of its 2.5D implementation – the noise in z -direction was misinterpreted as an edge and therefore was hardly smoothed; a real 3D implementation would have improved these results. In Fig. 6c the result of scanning the object 20 times plus averaging can be seen. Compared to the single scan in Fig. 6a there is a clear improvement in noise reduction, and as well large singular errors have disappeared. The result of the next step of processing, smoothing the averaged scans with the AD filter, is shown in Fig. 6d: The smoothing effect is clearly visible, nevertheless small structures like the eyebrows (width: between 3 and 5 mm) are preserved, but the mentioned problematic noise at the steeper edges remains. It can be reduced with the next step (Fig. 6e), where an additional gaussian filter was applied. The structures have flattened due to the combined effects of mixed pixels and the filter algorithms, as can be seen by comparison with the images of Fig. 1. Nevertheless the results obviously are much better than the comparable result from a single scan in 6b.



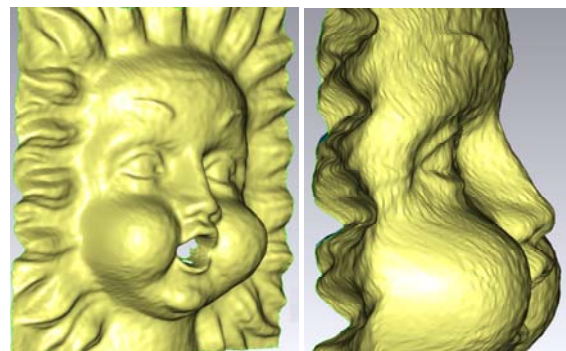
a) Single scan, no filter



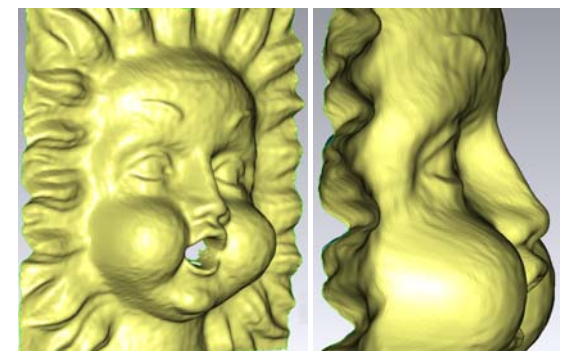
b) Single scan, gaussian and AD filtered



c) Average of 20 scans, no filter



d) Average of 20 scans, AD filtered



e) Average of 20 scans, gaussian and AD filtered

Figure 6. Comparison of single scan point clouds (a-b) to repeated and averaged scans (c-e), showing different states of the smoothing process

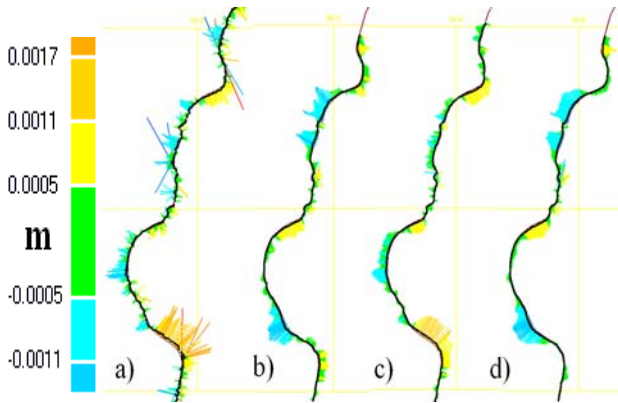


Figure 7. Reference vs. test models: Single scan (a), Average of 20 Scans (b), Single scan, AD-filtered (c), Average of 20 Scans, AD-filtered (d)

Until now, just relative comparisons amongst different smoothing steps were made. Now an absolute comparison vs. the reference model (Fig. 1), derived from the scans of the light section sensor is made: Sections through the test models (position of the sectioning plane see red line in Fig. 6a) are compared to a section through the reference model: In Fig. 7a, a single, unfiltered scan is compared to the reference scan, showing strong noise and outliers. Averaging 20 scans results in an outlier-free, but still noisy sectioning (Fig. 7b). In Fig. 7c, the single scan was carefully AD-filtered; afterwards he still shows some noise. Further iterations of the filter process would result in larger differences to the reference model. In Fig. 7d, the advantages of both processing steps are combined: after the averaging over 20 scans as a pre-smoothing step, low values for the AD filter parameters are sufficient. So on the one hand, the model is visually smooth (see also Fig. 6e) and on the other hand, it does not differ too much from the reference. The standard deviation is the same ($\sigma = 0.5$ mm) for all models except for the single scan ($\sigma = 0.7$ mm).

5. CONCLUSIONS

Repeated scanning, averaging and smoothing with an edge-preserving filter like the anisotropic diffusion filter is a good tool to reduce noise in point clouds of small-structured free form surfaces, where the application of linear smoothing filters would remove too much of the surface details. As expected, an angular and range resolution comparable to triangulation systems was not achieved (see discussion in section 1.2). But with the proposed workflow, visibly better results are achieved than by a single scan and non-curvature based linear filtering. The result is a compromise between a visually smooth surface and the preservation of the object geometry. The time, that had to be spent for the 19 additional scans was only about 10 minutes. As further steps, a 3D implementation of the ADF is necessary to improve the smoothing results. Determination of surface properties before and after the smoothing process, as i.e. is done in Nothegger and Dorninger (2009), could in future give a more qualitative tool to evaluate the results and also will enable a quicker choice of the proper filter parameters. Further filters will be investigated with respect to their applicability at the special requirements of small-structured free form surfaces.

REFERENCES

Adams, M. D., Probert, P. J., 1996. The Interpretation of Phase and Intensity Data from AMCW Light Detection Sensors for

Reliable Ranging. *The International Journal of Robotics Research* 1996; 15; pp. 441-458.

Amann, M.-C., Bosch, T., Lescure, M., Myllylä, R., Rioux, M., 2001. Laser ranging: a critical review of usual techniques for distance measurement. *Optical Engineering*, 40 (1), January 2001, pp. 10-19.

Atkins, P. W., 1990. *Physical Chemistry*. Oxford University Press, pp. 766-768

Böhler, W., Vicent, M. B., Marbs, A., 2003. Investigation Laser Scanner Accuracy. XIX CIPA Symp, Antalya, 30.9.-4.10.2003.

Clarenz, U., Diewald, U., Rumpf, M., 2004. Processing Textured Surfaces via Anisotropic Geometric Diffusion. In: *IEEE Transactions on Image Processing*, 13 (2), February 2004, pp. 248-261.

Gordon, S., Lichti, D., Stewart, M., Franke, J., 2003. Structural Deformation Measurement Using Terrestrial Laser Scanners. 11th FIG Symposium on Deformation Measurements, Santorini, Greece, 2003.

Guidi, G., Remondino, F., Morlando, G., Del Mastio, A., Ucheddu, F., Pelagotti, A., 2007. Performances Evaluation of a Low Cost Active Sensor for Cultural Heritage Documentation. In: *International Conference on Optical 3-D Measurement Techniques VIII*, Zurich, Switzerland, 2007, pp. 59-69.

Hebert, M., Krotkov, E., 1992. 3D Measurements from Imaging Laser Radars: How good are they? *Intl. Journal of Image and Vision Computing*, 10 (3), April 1992, pp. 170-178.

Lichti, D., Licht, G., 2006. Experiences with Terrestrial Laser Scanner Modelling and Accuracy Assessment. *International Archives of Photogrammetry, Remote Sensing*, Vol XXXVI, Part 5, pp. 155-160.

Nothegger, C., Dorninger, P., 2009. 3D Filtering of High-Resolution Terrestrial Laser Scanner Point Clouds for Cultural Heritage Documentation. *Photogrammetrie, Fernerkundung, Geoinformation*, 1/2009, pp. 53-63.

Perona, P., Malik, J., 1990. Scale-Space and Edge Detection Using Anisotropic Diffusion. In: *IEEE Transactions on Pattern Analysis and Machine Intelligence*, 12 (7), July 1990, pp. 629-639.

Pfeifer, N., Dorninger, P., Haring, A., Fan, H., 2007. Investigating terrestrial laser scanning intensity data: quality and functional relations. In: *International Conference on Optical 3-D Measurement Techniques VIII*, Zurich, Switzerland, 2007, pp. 328 - 337.

Wölfelschneider, H., Blug, A., Baulig, C., Höfler, H., 2005. Fast Distance Measurement for Laser Scanning. *tm Technisches Messen* 72 (2005) 7-8, pp. 455-467.

Zhang, X.-C., Xi, J.-T., Yan, J.-Q., 2006. A methodology for smoothing of point cloud data based on anisotropic heat conduction theory. *The International Journal of Advanced Manufacturing Technology*, 30 (1-2), August 2006, pp. 70-75.